THE JOURNAL OF PHYSICAL CHEMISTRY A
A JOURNAL OF THE AMERICAN CHEMICAL SOCIETY

pubs.acs.org/JPCA

Article

Theoretical Kinetics Predictions for Reactions on the NH_2O Potential Energy Surface

Stephen J. Klippenstein,* Clayton R. Mulvihill, and Peter Glarborg

Cite This: *J. Phys. Chem. A* 2023, 127, 8650−8662

Read Online

ACCESS | Metrics & More | Article Recommendations | Supporting Information

ABSTRACT: Recent modeling studies of ammonia oxidation, which are motivated by the prospective role of ammonia as a zero-carbon fuel, have indicated significant discrepancies among the existing literature mechanisms. In this study, high-level theoretical kinetics predictions have been obtained for reactions on the NH_2O potential energy surface, including the NH_2 + O, HNO + H, and NH + OH reactions. These reactions have previously been highlighted as important reactions in NH_3 oxidation with high sensitivity and high uncertainty. The potential energy surface is explored with coupled cluster calculations, including large basis sets and high-level corrections to yield high-accuracy (∼0.2 kcal/mol 2σ uncertainty) estimates of the stationary point energies. Variational transition state theory is used to predict the microcanonical rate constants, which are then incorporated in master equation treatments of the temperature- and pressure-dependent kinetics. For radical−radical channels, the microcanonical rates are obtained from variable reaction coordinate transition state theory implementing directly evaluated multireference electronic energies. The analysis yields predictions for the total rate constants as well as the branching ratios. We find that the NO + H_2 channel contributes 10% of the total NH_2 + O flux at combustion temperatures, although this channel is not included in modern NH_3 oxidation mechanisms. Modeling is used to illustrate the ramifications of these rate predictions on the kinetics of NH_3 oxidation and NO_x formation. The present results for NH_2 + O are important for predicting the chain branching and formation of NO in the oxidation of NH_3 and thermal $DeNO_x$.

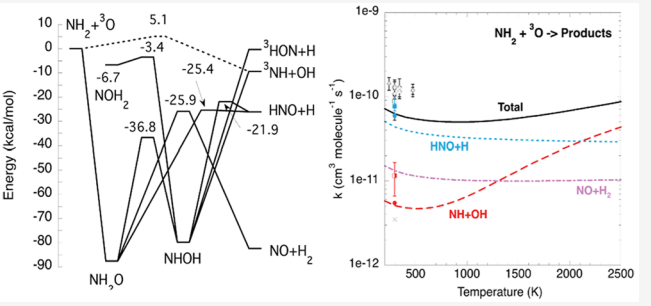

1. INTRODUCTION

The proposed use of ammonia as a sustainable fuel has attracted a great deal of attention in recent years.[1−5] These studies include a number of combined experimental and modeling studies investigating the oxidation of ammonia (see, e.g., refs 6−16 for a partial listing of the studies since 2015). The low burning velocity of ammonia presents significant challenges for its direct use as a fuel. Thus, more recent modeling studies have focused on its combustion properties in mixtures with H_2,[17−23] CH_4,[17,21,24−28] and CO[17,29,30] as well as a great variety of other fuels such as ethers, alcohols, larger alkanes, amines, etc.

One general conclusion from these studies[1−5] is that there is substantial variation in the predictions among the various models. Such variations are generally indicative of the fact that the available elementary reaction rate data are not extensive enough and/or are too inaccurate to reliably reproduce the rate constants and corresponding chemical conversions over the full range of conditions of relevance to the simulations. As a result, one finds that different groups adjust different aspects of the mechanism in order to obtain agreement for the particular experiments on which they are focused. Of course, such a process does not necessarily lead to a physically reliable mechanism that can automatically predict the behavior for arbitrary fuel mixtures. The best route out of this dilemma is to obtain more and better rate data for the key reactions over a wide range of temperatures and pressures. Here we employ high-level theory to improve the kinetic descriptions for the reactions occurring on the NH_2O potential energy surface (PES).

The reactivity of ammonia is largely governed by the fate of the amino radical NH_2, with the reaction of NH_2 with O showing high sensitivity in many of the prior modeling studies. In particular, the reaction generally shows up among the most sensitive reactions for laminar burning velocities of ammonia, both alone and in mixtures.[9,11,13,20,25,29−32] Meanwhile, NO, a key pollutant in NH_3 oxidation, is also particularly sensitive to this reaction.[13,24,26,33] Ignition delays generally do not show high sensitivity to this reaction, although it does show up at 10 atm and 1600 K in a 30:70 mixture of NH_3 and H_2,[23] at least for the mechanism of Otomo et al.[17] Also, under fuel-lean conditions, OH* shows some sensitivity to it.[7]

Received: August 1, 2023
Revised: September 18, 2023
Published: October 9, 2023

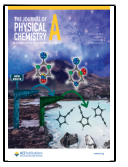

There are a number of possible product channels for the NH_2 + O reaction:

$$NH_2 + O(^3P) \rightarrow HNO + H \quad (\Delta H = -26.1 \text{ kcal/mol}) \tag{R1a}$$

$$NH_2 + O(^3P) \rightarrow HN + OH \quad (\Delta H = -9.4 \text{ kcal/mol}) \tag{R1b}$$

$$NH_2 + O(^3P) \rightarrow H_2 + NO \quad (\Delta H = -82.4 \text{ kcal/mol}) \tag{R1c}$$

$$NH_2 + O(^3P) \rightarrow HON(^3A'') + H \quad (\Delta H = -0.5 \text{ kcal/mol}) \tag{R1d}$$

$$NH_2 + O(^3P) \rightarrow H_2O + N(^4S) \quad (\Delta H = -48.8 \text{ kcal/mol}) \tag{R1e}$$

$$NH_2 + O(^3P) \rightarrow H_2NO \quad (\Delta H = -87.6 \text{ kcal/mol}) \tag{R1f}$$

$$NH_2 + O(^3P) \rightarrow HNOH \quad (\Delta H = -79.9 \text{ kcal/mol}) \tag{R1g}$$

A schematic plot of the reaction paths connecting these channels is provided in Figure 1. This diagram is based on the high-level electronic structure evaluations summarized below. It is important to understand both the overall reaction rate and the branching among these channels.

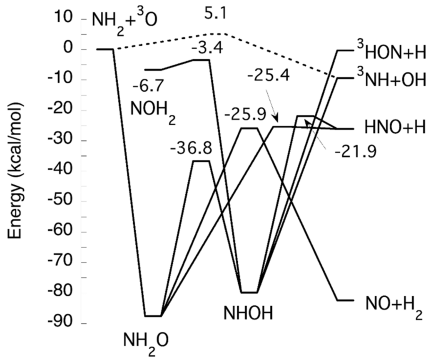

Figure 1. Schematic diagram of the key stationary points on the potential energy surface for the reaction of NH_2 with $O(^3P)$. The solid lines denote reactions on the ground doublet state, while the dashed line denotes reaction on the ground quartet state. For simplicity, the long-range minima (and their connections) in the entrance (NH_2 + O) and exit channels (NH + OH, HNO + H, and NO + H_2) are not illustrated.

Four separate experimental studies have measured the room-temperature rate constant,[34−37] with the three most recent studies in reasonable accord, with measured rate constants of 8.8 ± 1.3, 6.5 ± 1.3, and 12 ± 3 ($\times 10^{-11}$ cm^3 $molecule^{-1}$ s^{-1}). The rate constant is observed to be independent of pressure for pressures of a few Torr, with HNO + H expected to be the dominant products and only a minor contribution from the NH + OH product channel. The internal state distributions for both the HNO and OH products were observed in crossed-beam experiments of Patel-Misra and Dagdigian.[38,39] The study of Inomata and Washida also examined the temperature dependence over the temperature range from 242 to 473 K. There do not appear to be any measurements at the higher temperatures of relevance to combustion.

The H + HNO and NH + OH reactions, which take place on the same NH_2O PES, are also of general relevance to NH_3 oxidation and NO_x chemistry. For example, the H + HNO reaction routinely appears in sensitivity analyses of laminar burning velocities for ammonia.[20,25,26,29−31] Meanwhile, NO_x profiles for ammonia commonly show sensitivity to the NH + OH reaction.[24−26] The H + HNO reaction has been studied experimentally at both room temperature[40] and near 2000 K, with a variation of a factor of 3 in the reported rate constants from different studies.[41−43] Meanwhile, the reverse reaction, H_2 + NO, has been studied over a wide range of high temperatures (1760−4000 K).[44−46] The NH + OH reaction did not appear to have been studied experimentally. Interestingly, optimized values of the rate constants for the H + HNO and NH + OH reactions were recently reported in the model optimization study of Kovacs et al. for $H_2/O_2/NO_x$ combustion.[47]

The NH_2 + O reaction has been the subject of only a few prior theoretical analyses.[48−51] The studies of Walch[49] and of Yang et al.[50] examined only the PES, while the study of Bozelli and Dean[48] simply presumed a value for the high-pressure capture rate constant. Meanwhile, the study of Duan et al. obtained canonical variational transition state theory (VTST) rate predictions, but only for the NH + OH product channel.[51] A number of theoretical studies have examined other aspects of the NH_2O PES and kinetics including the H + HNO reaction,[52−54] the NH + OH reaction,[55−58] the N + H_2O reaction,[59−61] and the decomposition of H_2NO into NO + H_2.[62,63] Each of these studies is limited in their expected accuracy due to limitations in the electronic structure methodologies and/or the statistical theoretical frameworks that were employed.

In this work, we employ a combination of high-level electronic structure theory and sophisticated VTST methods to obtain higher-quality rate predictions for the various reactions on the NH_2O PES. In this analysis, the radical−radical channels are each treated with variable reaction coordinate transition state theory (VRC-TST), which has generally agreed with experimental observations to within about 20% in prior studies.[64] Multireference electronic structure methods are employed to predict the requisite interaction energies for these VRC-TST calculations. The remaining channels are treated with VTST. The stationary point properties (energies, geometries, and vibrational frequencies) are treated with a modestly improved version of the ANL1 method,[65] which employs a CCSD(T)/CBS analysis combined with a variety of additional corrections to obtain 2σ uncertainties for the stationary point energies of ~0.2 kcal/mol. Overall, we expect 2σ uncertainties of about a factor of 1.5 or less for each of the rate constants examined here.

The analysis includes an examination of the pressure dependence of the kinetics through master equation simulations for pressures of up to 100 atm. For the NH_2 + O reaction, there is little indication of stabilization or pressure dependence for the kinetics. In contrast, significant stabilization of the NH_2O and NHOH complexes is predicted at the highest pressures for the reactions of HNO with H and NH with OH. The implications of the updated rate coefficients for the NH_3 modeling predictions are discussed.

https://doi.org/10.1021/acs.jpca.3c05181
J. Phys. Chem. A 2023, 127, 8650−8662

2. METHODS

2.1. Stationary Points on the Potential Energy Surface. The rovibrational properties of the stationary points on the NH_2O PES were obtained at the complete basis set (CBS) limit of explicit CCSD(T)-F12 calculations for the cc-pVTZ-F12 and cc-pVQZ-F12 basis sets. Higher accuracy estimates for the stationary point energies were then obtained from a composite approach that mimics the ANL1 approach.[65] The terms in the composite consist of (i) a CCSD(T) estimate for the CBS limit obtained from explicit calculations for the aug′-cc-pV5Z and aug′-cc-pV6Z basis sets,[65,66] (ii) the sum of CCSDTQ(P)/cc-pVDZ and CCSDT(Q)/cc-pVTZ corrections for the effect of higher-order excitations[67] [CCSDTQ(P)/DZ-CCSDT(Q)/DZ+CCSDT(Q)/TZ-CCSD(T)/TZ], (iii) a CCSD(T)/CBS core−valence correction from an extrapolations of results for the cc-pcVTZ and cc-pcVQZ basis sets, (iv) a CCSD(T)/aug-cc-pcVTZ-DK evaluation of scalar relativistic effects employing the Douglas−Kroll−Hess (DKROLL = 1) one-electron integrals,[68] (v) a CCSD/cc-pVTZ evaluation of the diagonal Born−Oppenheimer correction (DBOC),[69] and (vi) a B2PLYP-D3/cc-pVTZ[70]-based calculation of anharmonic zero-point corrections via second-order vibrational perturbation theory. For comparison purposes, the CCSD(T)/CBS limit was also evaluated from the extrapolation of CCSD(T)-F12b calculations for the cc-pVQZ-F12 and cc-pV5Z-F12 basis sets.[71−73]

The CBS extrapolations employed coefficients of 0.6 and 0.5 for the CCSD(T)-F12 energy and frequency extrapolation, respectively, 0.69 for the core−valence energies, and 1.2 for the CCSD(T) energy extrapolation. The results are only very weakly dependent on reasonable values for these extrapolation coefficients (i.e., there is typically an extrapolation uncertainty of a few hundredths of a kcal/mol). For example, the difference between the CCSD(T)/CBS(aug′-cc-pVnZ) and CCSD(T)-F12/CBS-F12(cc-pVnZ-F12) extrapolation limits is, at most, 0.03 kcal/mol.

The calculations were mostly performed with MOLPRO.[74,75] The DBOC evaluations were performed with CFOUR, as were the CCSDT(Q) calculations for singlet states.[76] For doublet and triplet states, the CCSDT(Q) calculations employed Kallay's MRCC extension to MOLPRO,[77] as did all the CCSDTQ(P) calculations. The anharmonicity corrections were obtained with Gaussian.[78] The coupled cluster calculations employ a restricted spin Hartree−Fock wave function within the unrestricted coupled cluster formalism, except for the CCSDT(Q) and CCSDTQ(P) calculations which employ an unrestricted spin wave function for both the HF and coupled-cluster components. The CCSDT(Q) correction was then taken as the difference between the UUCCSDT(Q)/cc-pVDZ result and the RUCCSD(T)/cc-pVDZ result.

The present analysis, which we label here as ANL1′, represents a modest improvement over the related ANL1 method through the use of more accurate CCSD(T)-F12/cc-pVQZ-F12 geometries and harmonic frequencies. Thus, we expect the final energy estimates to have similar or lower 2σ uncertainties of 0.2 kcal/mol for the minima, at least for the stationary points with not too large a higher-level correction. The expected uncertainties for ANL1′ predictions of the saddle point energies are less clear, but our experience from limited comparisons suggests that these energies typically have similar uncertainties, again at least when the higher-level correction is not too large.

2.2. Radical−Radical Interactions and VRC-TST. For radical−radical reactions, it is challenging to obtain accurate predictions for the transition-state partition functions at large radical−radical separations where the energetics are not well described with single reference methods and the interfragment motions are transitioning from nearly harmonic oscillators to nearly free rotors. Furthermore, the reaction coordinate itself is then ill-defined, as it makes a transition from a bonding-like coordinate at short separation to a center-of-mass separation at larger separations. Here, we implement direct CASPT2 VRC-TST to treat these complexities for the addition reactions.[79,80] This approach is based on a separation into the "conserved" vibrational modes of the fragments and the remaining "transitional modes" describing the relative motions of the two fragments. The transitional modes are generally of low enough frequency that classical phase space integral treatments of their contributions are appropriate. The transition state dividing surface (or equivalently the reaction coordinate) is then defined by a fixed distance between the pivot points on each of the fragments. Monte Carlo integration over the transitional coordinates with directly evaluated interaction energies provides the cornerstone for the direct VRC-TST approach.

The presence of multiple electronic states in the NH_2 + O and NH + OH reactions leads to a few additional complications for the VRC-TST calculations. It is helpful to briefly review the nature of these electronic states and particularly the state dependence of the interaction potentials. The NH_2 + O and NH + OH channels each involve the interaction of a doublet radical with a triplet radical. These interactions lead to both doublet and quartet states. Furthermore, the nearly degenerate electronic states of O ($^3P_2$, $^3P_1$, and $^3P_0$) and OH ($^2\Pi_{3/2}$ and $^2\Pi_{1/2}$), which are split only by their spin−orbit splittings, lead to the presence of multiple doublet and quartet states for the interacting radicals. The quartet states are repulsive for the addition reactions, while the two lowest doublet states are attractive for NH_2 + O and only the lowest doublet state is attractive for NH + OH. For the direct abstraction reactions, the situation is reversed, with the quartet states being lower-lying and the doublet states having high barriers.

Notably, at the intermediate separations typical of van der Waals molecules (e.g., ∼3 Å separation), the doublet and quartet states are nearly degenerate (cf. Figure 2, where the ground doublet and quartet distinguished coordinate minimum-energy paths are illustrated for both addition reactions). Although not illustrated, for the NH_2 + O case in the van der Waals region, the three nearly degenerate orientations for the lone pair of the O atom yield three nearly degenerate doublet states and three nearly degenerate quartet states. As the NO distance decreases, for the doublet state one orientation becomes repulsive while the other two remain attractive and lead to a chemical adduct. All three quartet states become repulsive. Meanwhile, for the NH···OH case, there are two nearly degenerate orientations of the OH radical orbital in the van der Waals region, with only one of them being attractive at shorter separation.

The MEP for the NH + OH addition shows a long-range minimum at a separation of about 3.1 Å, where the OH is oriented to form a hydrogen bond with the N. At shorter separations, the NH and OH reorient to allow for the

https://doi.org/10.1021/acs.jpca.3c05181
J. Phys. Chem. A 2023, 127, 8650−8662

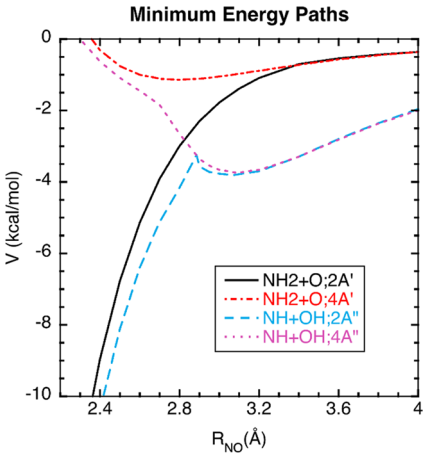

Figure 2. Plot of CASPT2-F12/cc-pVTZ-F12 distinguished coordinate minimum-energy paths for the lowest $^2A'$ and $^4A'$ states in the $NH_2 + O(^3P) \rightarrow H_2NO$ addition reaction and the lowest $^2A''$ and $^4A''$ states in the NH + OH → NHOH addition reaction.

formation of the NO chemical bond. The cusp on the distinguished coordinate minimum-energy path corresponds to the saddle point, where the NH and OH are in the midst of reorienting from the optimal hydrogen bond orientation to that which is optimal for covalent bond formation. The presence of the hydrogen bonded minimum on the PES then indicates that there are two transition states for the formation of the NHOH complex from NH and OH. The "outer" transition state separates the fragments from the hydrogen-bonded complex, while the "inner" transition state separates the hydrogen-bonded complexes from the NHOH complex.

As an aside, we note that a weaker hydrogen-bonded complex exists for the NH hydrogen bonded to the O. This complex plays a role in the abstraction to form $^4N + H_2O$, while the other hydrogen-bonded complex plays a role in the abstraction to form $^3O + NH_2$. In the present analysis, we assume a rapid equilibration of these long-range complexes (i.e., a rapid roaming assumption[81]) and evaluate the flux to form a global long-range complex with contributions from multiple electronic states. Then the various chemical reaction processes from this global complex are assumed to occur in competition, with statistical probabilities.[81]

For the NH_2 + O case, there is no long-range complex on the ground doublet state along the addition MEP. Nevertheless, a similar separation into inner and outer transition states and long-range complexes is appropriate due to the effects of entropic changes along the MEP. The centrifugal barriers again lead to a long-range/outer transition state, while the tightening of the intermolecular bending modes leads to a short-range/inner transition state. The MEP plot for the $^4A'$ state in the NH_2 + O reaction (cf. Figure 2) provides a good illustration of the presence of such a complex for the nonreactive states.

Thus, for both reactions, we employ two distinct VRC-TST treatments to obtain the reactive flux through these distinct transition states. For the outer TS, the reaction coordinate is taken to be the separation between the centers of mass of the two reacting radicals. Meanwhile, for the inner TS the reaction coordinate is represented in terms of a fixed distance between pivot points on each of the fragments. For the NH_2 fragment in the NH_2 + O reaction, we consider a pair of pivot points displaced above and below the N atom displaced by up to 1.5 bohr, while the O pivot point is just taken as the O atom itself. Pivot point to pivot point separations of 8 to 3.75 bohr are considered for the inner TS and from 20 to 8 bohr for the outer TS. For the NH + OH reaction, the inner TS pivot points are placed along the axis of the diatomic, with displacements from the center of mass of up to 0.5 bohr. Pivot point to pivot point separations of 6.5 to 4.0 bohr are considered for the inner TS and from 20 to 7 bohr for the outer TS.

We assume rapid intersystem crossing within the long-range region. We also assume that for the inner TS the repulsive states make no contribution to the reactive flux. Thus, for the NH_2 + O reaction, the contributions from the two lowest doublet states are included for the inner TS, while the contributions from all electronic states are included for the outer TS. For the NH + OH reaction, only the ground doublet state is assumed to contribute to the inner TS, while the contributions from all electronic states are again included for the outer TS. We further assume that the spin−orbit splittings are constant from the long-range minimum out to separated fragments and are negligible from the inner TS in to short separations. It is perhaps worth noting that for higher temperatures (e.g., ∼room temperature and above) the inner transition state provides the dominant bottleneck for both reactions, and the assumptions about intersystem crossing rates and interactions are then of little significance.

The interaction energies for such radical−radical channels in their low spin state cannot be treated effectively with standard single-reference-based methods such as CCSD(T). Instead, we employ complete active space second-order perturbation theory (CASPT2) and Davidson-corrected multireference singles and doubles configuration interaction (CI+QC) methods to explore these interactions. The energies from these multireference calculations for a specific geometry must be tied back to the energy framework for the overall system. These energy relations may be obtained from the multireference evaluations of the geometry-dependent energies relative to either separated fragments (NH_2 + O or NH + OH) or the quartet states at the same geometry. The latter spin-splitting-based approach requires an additional single-reference-based analysis of the quartet state interaction energy relative to infinite separation (e.g., via CCSD(T) or ANL1 calculations).

The spin-splitting approach is particularly effective because multireference methods are more consistent (and likely more accurate) in their prediction of these spin splittings than in their prediction of the interaction energies relative to separated fragments and because single-reference methods have high accuracy of high-spin interaction energies.[82] However, since the spin-splitting approach requires additional high-level calculations of the quartet state energies, we implement it only when deemed necessary, as indicated by significant differences between the CASPT2 and CI+QC analyses. For the NH_2 + O and NH + OH reactions, we find maximum differences of 6% between these two methods in the transition state region. Thus, we opted not to employ the spin-splitting methodology.

Notably, the dynamically corrected VRC-TST approach has been found to yield high accuracy (i.e., errors of ∼20%) a priori rate predictions when sufficient attention is paid to the generation of accurate interaction energies.[83] Here we employ direct sampling of CASPT2 energies within Monte Carlo-based phase space integration. The number of sampling points

https://doi.org/10.1021/acs.jpca.3c05181
J. Phys. Chem. A 2023, 127, 8650−8662

Table 1. Basis Set Convergence of Coupled Cluster Energies (kcal/mol) on the NH_2O Potential Energy Surface

	CCSD(T)-F12			CCSD(T)					
Stationary Point	QZ-F12	5Z-F12	CBS-F12[a]	AQZ	A5Z	A6Z	CBS[b]	Delta[c] CBS	T1[d] Diag.
Minima									
NH_2 + ^3O	0	0	0	0	0	0	0	0	0.008
^{4}[NH_2···O]; A′	−1.23	−1.23	−1.24	−1.08	−1.15	−1.19	−1.23	0.00	0.010
^{4}[NH_2···O];A″	−1.22	−1.22	−1.23	−1.04	−1.13	−1.17	−1.22	0.01	0.010
^{3}NH + OH	−7.74	−7.76	−7.77	−7.61	−7.69	−7.72	−7.75	0.02	0.008
^{4}[NH···OH];A′	−9.64	−9.66	−9.67	−9.46	−9.57	−9.61	−9.66	0.01	0.007
^{4}[OH···NH];linear	−11.33	−11.36	−11.37	−11.16	−11.26	−11.30	−11.35	0.02	0.008
HNO + H	−22.79	−22.89	−22.94	−21.11	−22.04	−22.44	−22.92	0.03	0.015
HNO···H;N side	−23.14	−23.25	−23.31	−21.36	−22.34	−22.77	−23.29	0.02	0.015
HNO···H;O side	−22.97	−23.07	−23.13	−21.22	−22.18	−22.60	−23.11	0.03	0.015
HNO···H;oop	−22.97	−23.07	−23.13	−21.23	−22.20	−22.61	−23.11	0.02	0.015
^{3}HON + H	2.82	2.78	2.75	4.01	3.35	3.09	2.78	0.03	0.025
H_2O + ^4N	−50.55	−50.54	−50.53	−50.67	−50.61	−50.57	−50.52	0.02	0.009
NO + H_2	−79.13	−79.20	−79.25	−77.57	−78.43	−78.80	−79.24	0.01	0.021
NH_2O	−91.60	−91.74	−91.82	−89.53	−90.73	−91.22	−91.81	0.01	0.030
NHOH;trans	−84.76	−84.84	−84.89	−82.99	−84.02	−84.43	−84.91	−0.01	0.025
NHOH;cis	−79.22	−79.31	−79.37	−77.39	−78.46	−78.88	−79.39	−0.02	0.025
NOH_2	−4.36	−4.46	−4.53	−8.78	−9.85	−10.28	−10.79	−0.01	0.016
Saddle Points									
NH_2···O = NH···OH;^{4}A″	7.89	7.88	7.88	8.20	8.05	7.97	7.89	0.01	0.050
NH_2···O═NH···OH;^{4}A′	8.35	8.34	8.33	8.68	8.51	8.43	8.34	0.01	0.054
NH_2O═NO + H_2	−23.28	−23.38	−23.45	−21.24	−22.38	−22.86	−23.43	0.02	0.036
NH_2O = HNO···H;oop	−22.20	−22.30	−22.36	−20.32	−21.36	−21.80	−22.33	0.03	0.021
NH_2O═NHOH	−37.49	−37.60	−37.66	−35.66	−36.73	−37.16	−37.67	−0.01	0.029
NHOH;cis = trans	−70.13	−70.21	−70.26	−68.36	−69.40	−69.80	−70.28	−0.02	0.017
NHOH;cis = HNO···H;N	−18.00	−18.07	−18.11	−16.09	−17.13	−17.57	−18.09	0.02	0.037
NHOH;trans = HNO···H;O	−17.03	−17.10	−17.15	−15.13	−16.17	−16.61	−17.13	0.02	0.035
NHOH = NOH_2	−4.36	−4.46	−4.53	−2.87	−3.75	−4.11	−4.54	−0.01	0.025
HNO···H;N = oop	−22.97	−23.07	−23.13	−21.23	−22.20	−22.61	−23.11	0.02	0.015
HNO···H;O = oop	−22.91	−23.02	−23.08	−21.18	−22.14	−22.55	−23.05	0.03	0.015
HNO···H;N = O	−22.91	−23.01	−23.07	−21.18	−22.13	−22.54	−23.04	0.03	0.015
HNO···H;N = H_2 + NO	−22.62	−22.72	−22.78	−20.87	−21.83	−22.24	−22.74	0.04	0.024
NH···OH = H_2O···^4N	−8.04	−8.04	−8.05	−7.84	−7.95	−7.99	−8.04	0.01	0.026

[a]The estimated CCSD(T)-F12/CBS-F12 limit obtained as CCSD(T)-F12/QZ-F12 + [CCSD(T)-F12/QZ-F12 − CCSD(T)-F12/TZ-F12] × 0.6. [b]The estimated CCSD(T)/CBS limit obtained as CCSD(T)/aug-cc-pV6Z + [CCSD(T)/aug-cc-pV6Z − CCSD(T)/aug-cc-pV5Z] × 1.2. [c]The difference between the CCSD(T)/CBS and CCSD(T)-F12/CBS-F12 limits. [d]The T1 diagnostic.

is chosen to yield convergence of the phase space integrals to ±5% at the 1σ level. The pivot point locations and separations are expected to yield a similar level of convergence for the dividing surface minimization within the VRC-TST approach. For each of these VRC-TST calculations, we append a dynamical recrossing correction factor of 0.85 in keeping with the expectations from dynamical simulations for simple model systems.[84]

For the NH_2 + O reaction, the direct sampling for the inner transition state employed a two-state average of the IPEA-shifted RS2/cc-pVQZ energies for a (5e, 4o) active space. For the outer transition state, we employ a three-state average instead of a two-state average to account for the additional near degeneracy of the states. The four active orbitals correlate with the NH_2 radical orbital and the O p orbitals in both cases.

For the NH + OH reaction, the direct sampling for the inner transition state employed the IPEA-shifted RS2-F12/cc-pVTZ-F12 energies for a (3e, 3o) active space. For the outer transition state, we instead employ a two-state average of the IPEA-shifted RS2/cc-pVQZ energies for a (5e, 4o) active space. The three active orbitals for the inner transition state correlate with the NH radical orbital and the OH radical orbital. The additional orbital for the outer transition state allows for coupling of the two nearly degenerate OH states. The RS2-F12 methodology is replaced with the RS2 methodology for the long-range calculations due to convergence problems with the former method.

Within VRC-TST, one-dimensional corrections to the interaction energies are commonly incorporated to account for limitations in the methodology employed in direct sampling. These corrections account for the effects of structural relaxation away from the asymptotic geometries, for limitations in the basis set used in the direct orientational sampling, and for limitations in the electronic structure method (e.g., the active space and the choice of CASPT2 versus CI +QC, etc.). For both the NH_2 + O and NH + OH reactions, the one-dimensional corrections are estimated to be 3% or less and so are simply ignored. Notably, when these corrections are small, the predictions are generally expected to have higher accuracy.

2.3. Variational Transition State Theory with Single Reference Wave Functions. For the remaining nonradical−radical transition states, we implemented variational transition state theory using either the POLYRATE code with internal-

https://doi.org/10.1021/acs.jpca.3c05181
J. Phys. Chem. A 2023, 127, 8650−8662

Table 2. Components of the ANL1′ Energies for the Stationary Points on the Potential Energy Surface for the Reaction of NH_2 with $O(^3P)$[a]

Stationary Point	CCSD(T) CBS[b]	T(Q) DZ[c]	T(Q) TZ[d]	Q(P) DZ[e]	HLC[f]	CV CBS[g]	Rel.[h]	BO[i]	E_0 Har[j]	E_0 Anh[k]	Total[l] ANL1′
NH_2 + ^3O	0	0	0	0	0	0	0	0	0	0	0
^{4}[NH_2···O];A″	−1.22	−0.03	−0.04	0.00	−0.04	0.00	0.00	*−0.07*	0.56	*−0.09*	−0.87
^{4}[NH_2···O];A′	−1.23	−0.01	−0.02	0.00	−0.02	0.00	0.00	0.04	0.55	−0.09	−0.76
^{3}NH + OH	−7.75	−0.01	−0.04	0.00	−0.04	0.06	0.04	0.03	−1.96	0.08	−9.42
^{4}[OH···NH];linear	−11.35	−0.08	−0.06	0.00	−0.06	0.03	0.06	0.01	−0.30	*−0.05*	−11.39
^{4}[NH···OH];A′	−9.66	−0.07	−0.05	0.00	−0.05	0.05	0.05	0.11	−1.09	0.08	−10.37
HNO + H	−22.92	−0.71	−0.36	0.05	−0.32	−0.07	0.12	0.06	−3.26	0.03	−26.12
HNO···H;N	−23.29	−0.72	−0.37	0.05	−0.32	−0.07	0.12	0.06	−2.78	*−0.03*	−26.08
HNO···H;O	−23.11	−0.72	−0.37	0.05	−0.32	−0.07	0.12	0.06	−2.99	*−0.06*	−26.14
HNO···H;oop	−23.11	−0.71	−0.37	0.05	−0.32	−0.07	0.12	−0.06	−3.00	*−0.03*	−26.24
^{3}HON + H	2.78	−0.41	−0.19	0.07	−0.11	−0.07	0.14	−0.08	−3.30	0.06	−0.36
H_2O + ^{4}N	−50.52	−0.06	0.07	0.02	0.09	−0.06	0.12	−0.13	1.48	−0.02	−48.82
NO + H_2	−79.24	−0.68	−0.34	0.06	−0.28	−0.08	0.04	−0.06	−2.97	−0.10	−82.44
NH_2O	−91.81	−0.39	−0.09	0.02	−0.07	−0.49	0.30	−0.08	4.82	−0.50	−87.61
NHOH;trans	−84.91	−0.48	−0.17	0.05	−0.12	−0.18	0.22	−0.08	5.03	−0.10	−79.90
NHOH;cis	−79.39	−0.47	−0.16	0.05	−0.11	−0.14	0.21	−0.06	4.63	−0.09	−74.73
NOH_2	−10.79	−0.3	−0.18	0.04	−0.15	0.09	0.15	*0.04*	4.05	−0.16	−6.68
NH_2···O = NH···OH;^{4}A″	7.89	−0.55	−0.69	0.01	−0.69	0.09	0.00	*0.22*	*−2.67*		5.06
NH_2···O = NH···OH;^{4}A′	8.34	−0.44	−0.51	−0.01	−0.52	0.08	0.00				5.68[m]
NH_2O = NO + H_2	−23.43	−1.18	−0.87	0.11	−0.76	0.07	0.08	0.09	−2.13	−0.09	−25.94
NH_2O = HNO···H;oop	−22.33	−1.38	−1.04	0.09	−0.95	−0.06	0.13	0.23	−2.49	−0.13	−25.37
NH_2O = NHOH	−37.67	−0.89	−0.49	0.07	−0.42	−0.08	0.14	−0.01	1.10	−0.04	−36.76
NHOH;cis = trans	−70.28	−0.40	−0.11	0.04	−0.07	−0.12	0.22	0.01	3.28	−0.04	−66.78
NHOH;cis = HNO···H;N	−18.09	−2.50	−2.27	0.17	−2.10	−0.04	0.11	0.14	−1.96	−0.19	−21.91
NHOH;trans = HNO···H; O	−17.13	−2.01	−1.75	0.11	−1.64	−0.04	0.12	0.13	−1.88	−0.19	−20.40
NHOH = NOH_2	−4.54	−0.94	−0.71	0.09	−0.61	0.18	0.09	*0.04*	1.31	−0.10	−3.44
HNO···H;N = oop	−23.11	−0.72	−0.37	0.05	−0.32	−0.07	0.12	−0.04	−3.06	*−0.05*	−26.30
HNO···H;O = oop	−23.05	−0.72	−0.37	0.05	−0.32	−0.07	0.12	*0.01*	−3.10	*−0.05*	−26.22
HNO···H;N = O	−23.04	−0.71	−0.37	0.05	−0.32	−0.07	0.12	0.06	−3.11	*−0.04*	−26.17
HNO···H;N = H_2 + NO	−22.74	−0.86	−0.52	0.07	−0.46	−0.05	0.11	*0.12*	−3.41		−26.20
NH···OH = H_2O···^{4}N	−8.04	−0.25	−0.30	0.00	−0.30	0.08	0.04	0.05	−1.12	*−0.07*	−9.07

[a]All are expressed in kcal/mol relative to NH_2 + $O(^3P)$. [b]The estimated CCSD(T)/CBS limit obtained as CCSD(T)/aug-cc-pV6Z + [CCSD(T)/aug-cc-pV6Z − CCSD(T)/aug-cc-pV5Z] × 1.2. [c]The CCSDT(Q)/cc-pVDZ correction given by the difference between the UUCCSDT(Q)/cc-pVDZ and RUCCSD(T)/cc-pVDZ energies. [d]The CCSDT(Q)/cc-pVTZ correction given by the difference between the UUCCSDT(Q)/cc-pVTZ and RUCCSD(T)/cc-pVTZ energies. [e]The CCSDTQ(P)/cc-pVDZ correction given by the difference between the UUCCSDTQ(P)/cc-pVTZ and UUCCST(Q)/cc-pVDZ energies. [f]The full higher-level correction (HLC) given by the sum of the CCSDT(Q)/cc-pVTZ and CCSDTQ(P)/cc-pVDZ corrections. [g]The CBS limit of the core−valence correction evaluated as CCSD(T,full)/cc-pcVQZ −CCSD(T)/cc-pcVQZ + {[CCSD(T,full)/cc-pcVQZ − CCSD(T)/cc-pcVQZ] − [CCSD(T,full)/cc-pcVTZ − CCSD(T)/cc-pcVTZ]} × 0.69. [h]The relativistic correction from CCSD(T)/aug-cc-pwCvqz-dk calculations. [i]The diagonal Born−Oppenheimer correction (DBOC) from CCSD/cc-pVTZ or HF/TZ calculations (italics). [j]The harmonic zero-point energy (ZPE) correction from CCSD(T)-F12/CBS-F12 calculations. [k]The anharmonic ZPE correction evaluated at the CCSD(T)/cc-pVQZ level or the B2PLYP-D3/cc-pVTZ level (in italics). [l]The total energy given by the sum of the CCSD(T)/CBS, HLC, core−valence, relativistic, DBOC, harmonic ZPE, anharmonic ZPE, and spin−orbit corrections (−0.22 for O, −0.11 for OH, and −0.17 for NO, respectively). [m]The ZPE and DBOC corrections for this excited electronic state were presumed to be equivalent to those for the ground state.

coordinate-based reaction path frequencies or distinguished coordinate minimum-energy path evaluations. The POLYRATE-based evaluations were used when the simpler distinguished coordinate evaluations suggested significant variational effects (i.e., for NH_2O = HNO···H, HNOH = HNO···H, and HNO···H = H_2 + NO). The reaction path was evaluated at either the CCSD(T)/cc-pVQZ level (for NH_2O = HNO···H, HNOH = HNO···H, and HNO···H = H_2 + NO) or the CCSD(T)-F12/cc-pVQZ-F12 level (for NH_2O = NHOH, NH_2O = NO + H_2, NHOH = NOH_2 → ^{4}N + H_2O, and NH + OH = H_2O + ^{4}N). For the NH_2 + ^3O → NH + OH channel, the reaction path was explored at the CI+QC/cc-pVQZ level due to convergence difficulties along the reaction path for coupled cluster methods. The reaction path energies were employed as shifts to the ANL1′ saddle point energies. Similarly, the reaction path frequencies were employed as shifts to the anharmonically corrected CCSD(T)-F12/CBS limit frequencies at the saddle point. The roaming channels connecting the three HNO···H complexes were treated with conventional transition state theory, and no anharmonicity corrections were included.

The two abstraction reactions, NH_2 + ^3O → NH + OH and NH + OH → ^{4}N + H_2O (for simplicity, not shown in Figure 1), proceed from quartet van der Waals complexes. Importantly, for such high-spin quartet states, single-reference-based method methodologies should be generally

https://doi.org/10.1021/acs.jpca.3c05181
J. Phys. Chem. A 2023, 127, 8650−8662

appropriate, and their saddle point geometries and energy properties were readily evaluated at the ANL1′ level. For the $NH_2 + O \rightarrow NH + OH$ reaction, there are two reactive electronic states. For simplicity, the rovibrational properties of the excited state were presumed to be equivalent to those of the ground state. Furthermore, due to some convergence failures in the CCSD(T)-F12 calculations, the vibrational frequencies for that channel were instead evaluated at the UCCSD(T)/cc-pVQZ level.

The reaction from HNO to form the set of HNO···H complexes was treated with VRC-TST employing a center-of-mass to center-of-mass reaction coordinate with directly evaluated CCSD(T)/cc-pVTZ energies. The distribution of the overall reactive flux into distinct minima was simply presumed to be partitioned equally. The significance of the decomposition of NHOH to ^{3}HON + H was explored with a simple phase space theory model, with the room-temperature reverse rate set to 3×10^{-10} cm^3 molecule^{-1} s^{-1}. Since the branching to this channel was predicted to be negligible, its role was not explored further.

2.4. Thermal Rate Constants. The full temperature and pressure dependences of the set of phenomenological rate constants for the reactions on the NH_2O potential energy surface were predicted through the implementation of these microcanonical RRKM rates within the master equation employing the MESS master equation system solver.[85,86] Asymmetric Eckart tunneling corrections were included for all of the tight transition states. The energy transfer was represented with Lennard-Jones collisions rates and a temperature-dependent $[\langle \Delta E_{down} \rangle = 100(T/298)^{0.85}]$ exponential down formula with the bath gas taken to be N_2.

3. RESULTS AND DISCUSSION

3.1. Potential Energy Surface. The various components of the stationary point energies on the NH_2O potential energy surface are provided in Tables 1 and 2, with the overall ANL1′ energies illustrated schematically in Figure 1. The energetics of the stable minima are compared with active thermochemical table (ATcT) values[87,88] in Table 3, while the barrier energies are compared with those from prior studies in Table 4.

The detailed results reported in these tables are useful for providing some indication of the expected accuracy of the final predictions for various stationary point energies. The small differences between the estimated CBS limit for the CCSD(T)-F12 and CCSD(T)/aug-cc-pVNZ series (0.04 kcal/mol or less) together with the small magnitude of the difference between the CCSD(T)-F12 results for the cc-pVQZ-F12 and cc-pV5Z-F12 basis sets (0.07 kcal/mol or less) indicate that the results are well converged with respect to the basis set. Although not reported here, the harmonic zero-point energy shows even better convergence with respect to the basis set size.

The T1 diagnostic is often taken to provide some indication of multireference character. All of the minima except NH_2O bear T1 diagnostics of 0.025 or lower, which suggests that there is little concern about multireference effects for these species. The T1 diagnostic of 0.030 for NH_2O suggests some minor concern, but the small magnitude of the higher-level correction (HLC, cf. Table 2, footnote f) (−0.07) suggests that the treatment of this species should be adequate. Notably, the T1 diagnostics for the NH_2···O = NH···OH (0.050), NHOH;cis = HNO···H;N (0.037), NHOH;trans = HNO···H;O (0.035), and NH_2O = NO + H_2 (0.036) saddle points are large enough to cause more significant concern. Furthermore, the HLCs of −0.69, −2.10, and −0.95 kcal/mol are large enough to indicate significantly increased uncertainty in the barrier height predictions. Note, however, that these same HLCs appear to be well converged with respect to the level of excitation (i.e., the CCSDTQ(P) corrections are each less than 0.17 kcal/mol) and reasonably well converged with respect to the basis set (i.e., the difference between the CCSDT(Q)/cc-pVTZ and CCSDT(Q)/cc-pVDZ corrections is each 0.35 kcal/mol or less).

Interestingly, there is a consistent 0.3 kcal/mol difference between the CCSDT(Q)/DZ and CCSDT(Q)/TZ corrections for all stationary points containing a NO bond. For HNO + H, we were able to evaluate the CCSDT(Q) correction for the larger cc-pVQZ basis, finding only a 0.03 kcal/mol difference from the CCSDT(Q)/TZ correction. This small difference suggests that the CCSDT(Q)/cc-pVTZ corrections are likely well converged with respect to the basis set.

The average absolute values of the HLC, core−valence, relativistic, DBOC, and anharmonic corrections are 0.40, 0.09, 0.11, 0.07, and 0.09 kcal/mol, respectively. Clearly, the higher-level correction for quadruple and pentuple excitations is of considerable importance for making accurate predictions of the kinetics. In contrast, the remaining corrections are only of minor significance.

Taken together, the small magnitude of the various corrections together with their convergence behavior strongly suggests that the predictions should be accurate (2σ) to within about 0.1 or 0.2 kcal/mol. Notably, the predicted reaction energies all agree with the ATcT values to within 0.12 kcal/mol, aside from that for NH_2O, which differs by −0.35 kcal/mol. The NH_2O radical is only weakly nonplanar. As a result, the anharmonic correction for this radical is quite large and difficult to determine accurately. However, it is also worth noting that the top contributors to the provenance of the ATcT value are largely theoretical. In principle, the challenge of accounting for correlations in such theoretical estimates could result in an underestimate of the ATcT error bars.

A select set of literature stationary point energies are compared with the present best estimate values in Table 4. This comparison is of interest, as it illustrates the magnitude of errors that might be expected with other commonly used electronic structure methods. The early multireference

Table 3. Comparison with ATcT Values[a]

Stationary Point	ATcT[b]	ATcT Unc.[c]	ANL1′[d]	Delta[e]
NH_2 + ^{3}O				
^{3}NH + OH	−9.50	0.05	−9.42	0.08
HNO + H	−26.24	0.04	−26.12	0.12
^{3}HON + H	−0.45	0.19	−0.36	0.09
H_2O + ^{4}N	−48.78	0.03	−48.82	−0.04
NO + H_2	−82.49	0.03	−82.44	0.05
NH_2O	−87.25	0.16	−87.61	−0.35
NHOH;trans	−79.95	0.19	−79.90	0.05
NHOH;cis	−74.68	0.41	−74.73	−0.05

[a]All values are in kcal/mol relative to NH_2 + ^{3}O. [b]ATcT values[87,88] from version TN 1.124. [c]ATcT uncertainties from individual component uncertainties. A direct ATcT calculation would obtain slightly different reaction uncertainties, but such values are not available through the web site. [d]ANL1′ values as reported in Table 2. [e]Difference between the ANL1′ and ATcT values.

https://doi.org/10.1021/acs.jpca.3c05181
J. Phys. Chem. A 2023, 127, 8650−8662

Table 4. Comparison of Literature Stationary Point Energies with the Present Best Estimates[a]

Stationary Point	Present[b] Work	Walch[c] CI+QC//CAS	Isegawa[d] CASPT2	Yang[e] G2	Asemani[f] CBS-QB3	Klippenstein[g] CCSD(T)// CCSD(T)	Homayoon[h] CCSD(T)-F12 //CCSD(T)
				Minima			
$NH_2 + O$	0	0			0	0	0
NH_2O	−87.61	7.8	0.0	0.0	−2.4	0.6	1.0
NHOH	−79.90	5.1	2.5	−0.6	−1.1	−0.1	0.0
NOH_2	−6.68		4.4		0.0		1.3
HNO + H	−26.12	3.4		−1.7	−1.7	0.0	0.2
^{3}HON + H	−0.36				−1.0		0.1
NH + OH	−9.42			0.0	−0.3	−0.4	−0.1
$NO + H_2$	−82.44			−2.5	−2.8	0.4	2.4
				Saddle Points			
$NH_2 + O = NH + OH$	5.06			1.6		0.4	
$NH_2O = NHOH$	−36.76	5.0	−3.6	0.7	−0.8	1.1	1.9
$NH_2O = NO + H_2$	−25.94	3.6	−2.9	0.0	−0.9	0.3	1.6
$NH_2O = HNO + H$	−25.37		−4.2	−1.2	−2.4	0.7	3.2
$H + HNO = NO + H_2$	−26.20		−4.3				
$NHOH = NOH_2$	−3.44		−0.8		0.2		1.8
NHOH = HNO + H	−21.91	5.1	−2.3	0.4	0.6	1.5	2.4

[a]All values are in kcal/mol relative to NH_2 + O and include zero-point corrections. The values are reported as errors relative to the present best estimate values. [b]Best estimates from the present work. [c]MRCI+QC/TZ//CAS/DZ calculations from ref 49. [d]CASPT2(13e,10o)/TZ calculations from ref 61. For this case, we used NH_2O as the reference because zero-point-corrected values are not provided for NH_2 + O. [e]G2 calculations from ref 50. [f]CBS-QB3 calculations from ref 58. [g]CCSD(T)/CBS//CCSD(T)/ATZ calculations from ref 55. [h]CCSD(T)-F12/AQZ//CCSD(T)/6-311+G(d,p) calculations with the UMP2/6-311+G(d,p) zero-point correction from ref 59.

configuration interaction values from Walch[49] show a systematic error of about 5 kcal/mol, suggesting a poor treatment of the NH_2 + O asymptote. As noted by Walch, this systematic error can be removed through the use of a different reference state, but random errors of 2 kcal/mol remain. The more recent CASPT2 analysis of Isegawa et al.[61] removes the systematic error but shows even larger random errors of about 3 kcal/mol. From our experience, such CASPT2 errors are fairly typical of attempts to describe large-scale chemical changes. Although not included in Table 4, related MRCI+Q calculations from Page and co-workers for the NH_2 + O abstraction[51] and the H + HNO additions and abstraction[52,53] show similar errors.

The CBS-QB3 method, which in large part aims to approximate the CCSD(T)/CBS result with simple inexpensive calculations, is commonly employed in combustion studies. For this system, the CBS-QB3 energies[58] are too low by 1.0 kcal/mol on average, with about 2 kcal/mol random deviations relative to that average error. The results for the G2 method[50] are similar in nature to those for the CBS-QB3 method. While the mean error is much smaller (−0.4 kcal/mol), the random errors are still about 2 kcal/mol. The CCSD(T)/CBS calculations from ref 55 also show a small average error of 0.4 kcal/mol, but now the deviation about that value is reduced to about 1 kcal/mol. This sort of reduction in error is typical of more quantitative efforts to reach the CCSD(T)/CBS limit. The more recent CCSD(T)-F12/aug-cc-pVQZ analysis of Hoyamoon and Bowman[59] is not as accurate as the CCSD(T)/CBS analysis from ref 7, with an average error of 1.4 kcal/mol and random deviations of about 2 kcal/mol from that average. These increased deviations appear to be indicative of a failure to include a CBS extrapolation and the limitation of the MP2 method for predicting zero-point energies.

3.2. Rate Predictions. The present ab initio TST-based master equation predictions for the rate constants for the reaction of NH_2 with $O(^3P)$ are illustrated in Figure 3 together

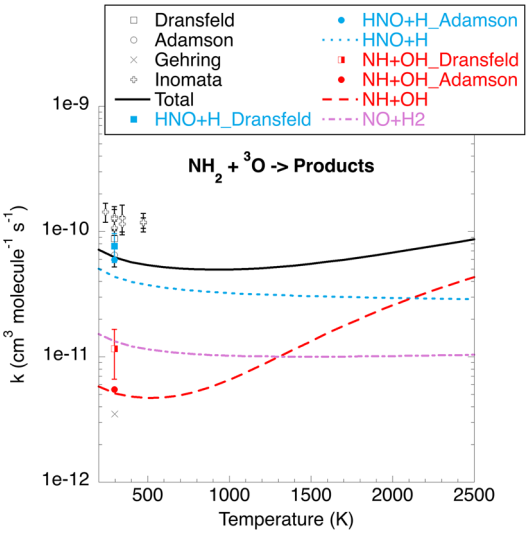

Figure 3. Plot of the rate constant for the reaction of NH_2 with $O(^3P)$. The black symbols and line denote the total rate constant, the blue symbols and line denote the rate for forming HNO + H, the red symbols and line denote the rate for forming NH + OH, and the purple line denotes the rate for forming NO + H_2.

with the available experimental data.[34−37] Note that the theoretical analysis indicates that there is essentially no pressure dependence for this reaction. These theoretical predictions are in remarkably good agreement with the room-temperature data of Adamson et al.[36] for both the total rate constant and the branching to the HNO + H and NH + OH channels. The predicted temperature dependence agrees with that observed by Inomata and Washida,[37] although their absolute value is somewhat higher. The data of Dransfeld et al.[35] is also in reasonable accord with the predictions, while the overall rate of Gehring et al.[34] is clearly too low. The good agreement between the a priori theoretical predictions and the

https://doi.org/10.1021/acs.jpca.3c05181
J. Phys. Chem. A 2023, 127, 8650−8662

Table 5. Modified Arrhenius Fits to the Master Equation's Predicted Rate Constants

Reaction	Pressure (bar)	A^a	n	E_a (cal/mol)	T range^b
$NH_2 + O = HNO + H$	*P*-independent	2.78×10^{13}	−0.065	−188	300−2500
$NH_2 + O = NH + OH$	*P*-independent	3.09×10^{3}	2.84	−2780	300−2500
$NH_2 + O = NO + H_2$	*P*-independent	2.38×10^{12}	0.112	−347	300−2500
$NH + OH = HNO + H$	*P*-independent	1.51×10^{14}	−0.314	−308	300−2500
$NH + OH = NO + H_2$	*P*-independent	3.43×10^{13}	−0.303	−336	300−2500
$NH + OH = {}^4N + H_2O$	*P*-independent	2.61×10^{7}	1.66	−945	300−2500
$HNO + H = NO + H_2$	*P*-independent	1.66×10^{10}	1.18	−446	300−2500
$HNO + H = NHOH$	0.01	7.01×10^{18}	−3.18	2600	300−2500
	0.1	7.09×10^{22}	−3.95	2487	300−2500
	1	4.89×10^{24}	−4.14	3141	300−2500
	10	3.57×10^{24}	−3.79	3702	300−2500
	100	1.03×10^{24}	−3.36	4710	400−2500
$HNO + H = HN_2O$	0.01	5.67×10^{23}	−4.59	5690	600−2500
	0.1	5.69×10^{25}	−4.80	4233	500−2500
	1	2.68×10^{27}	−4.94	4849	500−2500
	10	2.55×10^{27}	−4.63	5539	500−2500
	100	4.84×10^{25}	−3.87	5867	500−2500
$NHOH = H_2 + NO$	0.01	8.49×10^{25}	−4.99	53140	500−2500
	0.1	4.21×10^{27}	−5.20	55170	500−2500
	1	1.47×10^{28}	−5.12	56560	500−2500
	10	3.29×10^{27}	−4.69	57520	500−2500
	100	5.76×10^{25}	−3.95	58190	500−2500
$NHOH = NH_2O$	0.01	2.30×10^{25}	−5.13	39080	500−2500
	0.1	3.47×10^{26}	−5.15	41210	500−2500
	1	3.45×10^{27}	−5.13	43280	500−2500
	10	7.74×10^{27}	−4.93	45060	500−2500
	100	3.39×10^{26}	−4.26	45960	500−2500
$NH_2O = H_2 + NO$	0.01	1.57×10^{27}	−5.28	61560	500−2500
	0.1	1.79×10^{28}	−5.32	63290	500−2500
	1	1.42×10^{28}	−5.05	64350	500−2500
	10	4.66×10^{26}	−4.39	64830	500−2500
	100	1.65×10^{23}	−3.18	64220	500−2500

^{a}For bimolecular rate constants, the A factors has units of $cm^3\ mol^{-1}\ s^{-1}$. For the unimolecular reaction, the A factors have units of s^{-1}. ^{b}Temperature range over which the fit is valid, in K.

room-temperature experimental data lends confidence to the theoretical predictions for the higher temperatures of relevance to ammonia oxidation.

Fits of modified Arrhenius expressions to the results of the master equation calculations are reported in Table 5. The calculations were performed for temperature ranging from 300 to 2500 K and for pressure ranging from 0.01 to 100 atm. The complete MESS master equation input files are provided in the Supporting Information. For conciseness, we report the rates only for those channels with a branching fraction that is 10% or larger. Furthermore, we report the rates for only one direction, with the presumption that thermochemistry will generally be used to obtain the rates for the reverse direction. The forward direction is chosen here to correspond to the direction in which the reaction is exothermic. A comparison of the present rate constants with the corresponding values from Glarborg[10] and Stagni[13] is given in the SI.

3.3. Modeling Comparisons. It is important to establish reliable chemical kinetic models for the ignition and oxidation of ammonia to facilitate its use in engines and gas turbines. In this section, we discuss the impact of the novel findings related to reactions on the NH_2O potential energy surface on modeling predictions for ammonia oxidation and the use of ammonia to control NO (thermal $DeNO_x$). The calculations were conducted with the chemical kinetic model from Glarborg et al.,[10] with modifications according to more recent work.[16]

We emphasize here the impact of the rate constant and product branching ratio for the $NH_2 + O$ reaction. Compared to the available experimental data for this reaction, the present theoretical study offers novel information about the temperature dependence of the reaction as well as its product branching fraction. As shown in Figure 3, the only measurements for the rate constant of the $NH_2 + O$ reaction were obtained at temperatures of 250−500 K. The results from Dransfeld et al.,[35] Adamson et al.,[36] and Inomata and Washida[37] are essentially in agreement, but the extrapolation to combustion temperatures has been uncertain. Furthermore, the theoretical branching fraction is different from that derived in the low-temperature experimental work (Figure 3). Among the three product channels for $NH_2 + O$, i.e., HNO + H (R1a), NH + OH (R1b), and NO + H_2 (R1c), there is good agreement concerning R1a (fast, the major channel) and R1b (a minor channel). However, contrary to the present analysis, none of the experimental studies identified NO + H_2 (R1c) as an important channel. Accordingly, recent NH_3 oxidation mechanisms (e.g., refs 7, 10, and 13) do not contain the NO + H_2 channel, even though this channel contributes ∼10% of the total $NH_2 + O$ flux at combustion temperatures (see Figure 3).

https://doi.org/10.1021/acs.jpca.3c05181
J. Phys. Chem. A 2023, 127, 8650−8662

To understand the role of the NH_2 + O reaction in high-temperature amine chemistry, it is instructive to review the ammonia oxidation mechanism. Owing to the low reactivity of NH_2 with O_2, the key step in the presence of even small amounts of NO is the fast NH_2 + NO reaction. This reaction simultaneously removes NO and produces free radicals to sustain reaction. It has two product channels, $NH_2 + NO = N_2 + H_2O$ and $NH_2 + NO = NNH + OH$, with NNH rapidly dissociating to form N_2 + H. At higher temperatures, the chain branching cycle, involving $H + O_2 = O + OH$, occurs readily, leading to strong growth in the O/H radical pool. This promotes the reaction of NH_2 with the radical pool, leading to the formation of NO through $NH_2 + O = HNO + H$, HNO → NO or $NH_2 + OH = NH + H_2O$, $NH + O_2 = NO + OH$. Fast generation of chain carriers thus leads to the formation of NO, while at lower radical levels NO is mostly consumed by the NH_2 + NO reaction.

The NH_2 + O reaction is important both for the chain branching in the system and as a source of NO, either directly (R1c) or through HNO (R1a) or NH (R1b). The role of the reaction depends on the competition between R1 (leading to branching through the subsequent step $H + O_2 = O + OH$) and R1c (chain-terminating). The product channel to NO + H_2 (R1c) thus inhibits the reaction, leading to a decrease in NO formation (despite forming NO).

In their modeling study of high-temperature amine chemistry, Klippenstein et al.[89] adopted values of k_{1a} and k_{1b} based on the low-temperature measurements,[35−37] assuming the values to be independent of temperature. In the more recent modeling study by the same group,[10] a $T^{-0.5}$ temperature dependence for reaction R1a was adopted, based on unpublished data by Temps (cited by Miller et al.[90]).

Figure 4 compares the NO formation in the oxidation of NH_3 in a jet-stirred reactor (JSR) reported by Dagaut[91] with modeling predictions investigating the impact of the choice of rate constants for NH_2 + O. Use of the values we adopted in Klippenstein et al.[89] (i.e., with a direct, temperature-independent extrapolation of the low-temperature measurements) leads to enhanced chain branching and thereby a larger formation of NO. Better agreement with experiment is obtained by using the present values (due mainly to the terminating contribution from R1c) or the values from Miller et al. (negative temperature coefficient for R1a). The overprediction of NO indicates that the production of chain carriers is not captured accurately by the model, even with the present values of k_{1a}, k_{1b}, and k_{1c}. However, at high temperature, the JSR data, in particular, the selectivity for forming NO, may be affected by the finite mixing rates in the reactor.

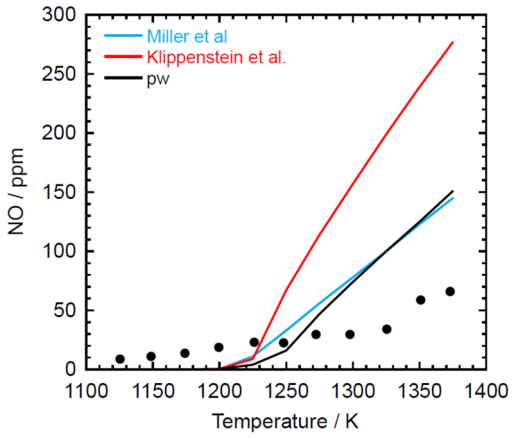

Figure 4. Impact of the choice of rate constants for the reaction of NH_2 with O for the prediction of the NO formation in the oxidation of NH_3 in a jet-stirred reactor. The black symbols denote the experimental data from Dagaut.[91] The lines denote modeling predictions with values of k_{1a}, k_{1b}, and k_{1c} from Miller et al.[90] (k_{1a} = 6.6×10^{14} $T^{-0.5}$ cm^3 mol^{-1} s^{-1}, k_{1b} = 6.8×10^{12} cm^3 mol^{-1} s^{-1}, k_{1c} = 0), Klippenstein et al.[89] (k_{1a} = 6.6×10^{13} cm^3 mol^{-1} s^{-1}, k_{1b} = 7.0×10^{12} cm^3 mol^{-1} s^{-1}, k_{1c} = 0), and the present work (pw, see Table 5). Conditions: an inlet mixture with 1000 ppm NH_3 and 12500 ppm O_2 in N_2, a nominal residence time of 0.1 s, and atmospheric pressure.

Figure 5 compares experimental results for NO in the thermal $DeNO_x$ process from Duo[92] with modeling predictions, investigating again the impact of the choice of rate constants for NH_2 + O. Similar to the results in Figure 4, a direct, temperature-independent extrapolation of the low-temperature measurements (Klippenstein et al.) leads to enhanced chain branching and overprediction of NO, while use of the present values or the values from Miller et al. improves the agreement with experiment at high temperatures. Interestingly, at temperatures below 1200 K, the current rate constants for NH_2 + O lead to a small increase in the predicted reactivity, slightly deteriorating the accuracy of the calculations. The different impact depending on temperature is due to the changes in the NH_2 consumption paths, with NH_2 + NO dominating below 1200 K, while NH_2 reactions with the radical pool become increasingly important at high temperatures.[10] The location of the thermal $DeNO_x$ temperature window depends primarily on the branching fraction of the NH_2 + NO reaction, while radical−radical reactions such as NH_2 + O have a significant effect on the width of the window.

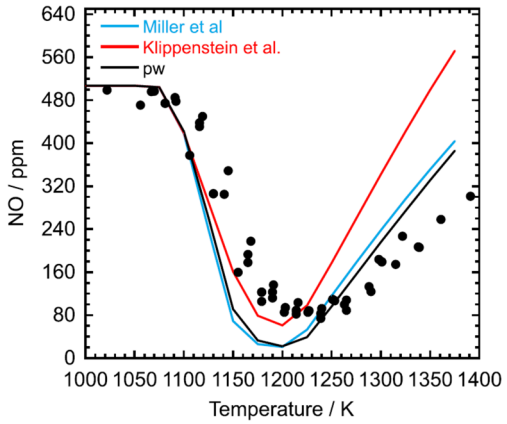

Figure 5. Impact of the choice of rate constants for the reaction of NH_2 with O for prediction of the NO reduction by NH_3 in a laminar flow reactor. Symbols denote the experimental data from Duo,[92] while lines denote modeling predictions with values of k_{1a}, k_{1b}, and k_{1c} from Miller et al.,[90] Klippenstein et al.,[89] and the present work (pw), respectively. Conditions: an inlet mixture with 832 ppm NH_3, 507 ppm NO, and 4.0% O_2 in N_2, a nominal residence time (s) of 92.7/T(K), and atmospheric pressure.

The modeling comparisons shown in this section illustrate the importance of employing accurate rate coefficients for the NH_2 + O reaction. The introduction of the third chain-terminating product channel to NO + H_2 facilitates a more accurate prediction of both the production of chain carriers

https://doi.org/10.1021/acs.jpca.3c05181
J. Phys. Chem. A 2023, 127, 8650−8662

and the formation of NO in the oxidation of NH_3 at high temperature.

4. CONCLUSIONS

The present analysis employed a combination of high-level electronic structure and transition state theory methods to obtain high-accuracy predictions for the kinetics of the reaction channels of relevance to the reaction of NH_2 with O as well as other reactions on the NH_2O potential energy surface. Inclusion of these rate predictions in our previously published model for nitrogen chemistry has a significant impact on NH_3 ignition and oxidation.

■ ASSOCIATED CONTENT

Supporting Information

The Supporting Information is available free of charge at https://pubs.acs.org/doi/10.1021/acs.jpca.3c05181.

The present rate constants for the NH_2O system are compared with the corresponding values from Glarborg[10] and Stagni;[13] note that this comparison does not highlight that a few reactions are not present in those mechanisms (PDF)

The mess input files for the present kinetics calculations (TXT)

The mess input files for the present kinetics calculations (TXT)

The mess input files for the present kinetics calculations (TXT)

The mess input files for the present kinetics calculations (TXT)

The mess input files for the present kinetics calculations (TXT)

The mess input files for the present kinetics calculations (TXT)

The mess input files for the present kinetics calculations (TXT)

The mess input files for the present kinetics calculations (TXT)

The mess input files for the present kinetics calculations (TXT)

The mess input files for the present kinetics calculations (TXT)

■ AUTHOR INFORMATION

Corresponding Author

Stephen J. Klippenstein − *Chemical Sciences and Engineering Division, Argonne National Laboratory, Lemont, Illinois 60439, United States;* orcid.org/0000-0001-6297-9187; Email: sjk@anl.gov

Authors

Clayton R. Mulvihill − *Chemical Sciences and Engineering Division, Argonne National Laboratory, Lemont, Illinois 60439, United States;* orcid.org/0000-0002-4256-1311

Peter Glarborg − *DTU Chemical Engineering, Technical University of Denmark, 2800 Lyngby, Denmark;* orcid.org/0000-0002-6856-852X

Complete contact information is available at: https://pubs.acs.org/10.1021/acs.jpca.3c05181

Notes

The authors declare no competing financial interest.

■ ACKNOWLEDGMENTS

This material is based on work supported by the U.S. Department of Energy, Office of Science, Office of Basic Energy Sciences, Division of Chemical Sciences, Geosciences, and Biosciences under contract no. DE-AC02-06CH11357. Support for S.J.K. and C.R.M. was provided by the Gas-Phase Chemical Physics Program of DOE-BES-CSGB as part of the Argonne-Sandia Consortium on High-Pressure Combustion Chemistry (FWP# 2009 ANL 59044).

■ REFERENCES

(1) Valera-Medina, A.; Xiao, H.; Owen-Jones, M.; David, W. I. F.; Bowen, P. J. Ammonia for Power. *Prog. Energy Combust. Sci.* **2018**, *69*, 63−102.

(2) Kobayashi, H.; Hayakawa, A.; Somarathne, K. K. A.; Okafor, E. C. Science and Technology of Ammonia Combustion. *Proc. Combust. Inst.* **2019**, *37*, 109−133.

(3) Elishav, O.; Lis, B. M.; Miller, E. M.; Arent, D. J.; Valera-Medina, A.; Dana, A. G.; Shter, G. E.; Grader, G. S. Progress and Prospective of Nitrogen-Based Alternative Fuels. *Chem. Rev.* **2020**, *120*, 5352−5436.

(4) Valera-Medina, A.; Amer-Hatem, F.; Azad, A. K.; Dedoussi, I.; De Joannon, M.; Fernandes, R. X.; Glarborg, P.; Hashemi, H.; He, X.; Mashurk, S.; McGowan, J.; Mounaim-Rouselle, C.; Ortiz-Prado, A.; Ortiz-Valera, J. A.; Rossetti, I.; Shu, B.; Yehia, M.; Xiao, H.; Costa, M. A Review on Ammonia as a Potential Fuel: From Synthesis to Economics. *Energy Fuels* **2021**, *35*, 6964−7029.

(5) Kang, L.; Pan, W.; Zhang, J.; Wang, W.; Tang, C. A Review on Ammonia Blends Combustion for Industrial Applications. *Fuel* **2023**, *332*, No. 126150.

(6) Hayakawa, A.; Goto, T.; Mimoto, R.; Arakawa, Y.; Kudo, T.; Kobayashi, H. Laminar Burning Velocity and Markstein Length of Ammonia/Air Premixed Flames at Various Pressures. *Fuel* **2015**, *159*, 98−106.

(7) Mathieu, O.; Petersen, E. L. Experimental and Modeling Study on the High-Temperature Oxidation of Ammonia and Related NOx Chemistry. *Combust. Flame* **2015**, *162*, 554−570.

(8) Song, Y.; Hashemi, H.; Christensen, J. M.; Zou, C.; Marshall, P.; Glarborg, P. Ammonia Oxidation at High Pressure. *Fuel* **2016**, *181*, 358−365.

(9) Nakamura, H.; Hasegawa, S.; Tezuka, T. Kinetic Modeling of Ammonia/Air Weak Flames in a Micro Flow Reactor with a Controlled Temperature Profile. *Combust. Flame* **2017**, *185*, 16−27.

(10) Glarborg, P.; Miller, J. A.; Ruscic, B.; Klippenstein, S. J. Modeling Nitrogen Chemistry in Combustion. *Prog. Energy Combust. Sci.* **2018**, *67*, 31−68.

(11) Mei, B.; Zhang, X.; Ma, S.; Cui, M.; Guo, H.; Cao, Z.; Li, Y. Experimental and Kinetic Modeling Investigation on the Laminar Flame Propagation of Ammonia Under Oxygen Enrichment and Elevated Pressure Conditions. *Combust. Flame* **2019**, *210*, 236−246.

(12) Dai, L.; Gersen, S.; Glarborg, P.; Levinsky, H.; Mokhov, A. Experimental and Numerical Analysis of the Autoignition Behavior of NH_3 and NH_3/H_2 Mixtures at High Pressure. *Combust. Flame* **2020**, *215*, 134−144.

(13) Stagni, A.; Cavallotti, C.; Arunthanayothin, S.; Song, Y.; Herbinet, O.; Battin-Leclerc, F.; Faravelli, T. An Experimental, Theoretical and Kinetic-Modeling Study of the Gas-Phase Oxidation of Ammonia. *React. Chem. Eng.* **2020**, *5*, 696−711.

(14) Manna, M. V.; Sabia, P.; Ragucci, R.; de Joannon, M. Ammonia Oxidation Regimes and Transitional Behaviors in a Jet Stirred Flow Reactor. *Combust. Flame* **2021**, *228*, 388−400.

(15) Abian, M.; Benes, M.; de Goni, A.; Munoz, B.; Alzueta, M. U. Study of the Oxidation of Ammonia in a Flow Reactor. Experiments and Kinetic Modeling Simulation. *Fuel* **2021**, *300*, No. 120979.

(16) Glarborg, P. The $NH_3/NO_2/O_2$ System: Constraining Key Steps in Ammonia Ignition and N_2O Formation. *Combust. Flame* **2022**, 112311.

(17) Otomo, J.; Koshi, M.; Mitsumori, T.; Iwasaki, H.; Yamada, K. Chemical Kinetic Modeling of Ammonia Oxidation with Improved Reaction Mechanism for Ammonia/Air and Ammonia/Hydrogen/Air Combustion. *Int. J. Hyd. Energy* **2018**, *43*, 3004−3014.
(18) Shrestha, K. P.; Seidel, L.; Zeuch, T.; Mauss, F. Detailed Kinetic Mechanism for the Oxidation of Ammonia Including the Formation and Reduction of Nitrogen Oxides. *Energy Fuels* **2018**, *32*, 10202−10217.
(19) He, X.; Shu, B.; Nascimento, D.; Moshammer, K.; Costa, M.; Fernandes, R. X. Auto-Ignition Kinetics of Ammonia and Ammonia/Hydrogen Mixtures at Intermediate Temperatures and High Pressures. *Combust. Flame* **2019**, *206*, 189−200.
(20) Han, X.; Wang, Z.; Costa, M.; Sun, Z.; He, Y.; Cen, K. Experimental and Kinetic Modeling Study of Laminar Burning Velocities of NH_3/air, NH_3/H_2/air, NH_3/CO/air and NH_3/CH_4/air Premixed Flames. *Combust. Flame* **2019**, *206*, 214−226.
(21) Li, R.; Konnov, A. A.; He, G.; Qin, F.; Zhang, D. Chemical Mechanism Development and Reduction for Combustion of $NH_3/H_2/CH_4$ Mixtures. *Fuel* **2019**, *257*, No. 116059.
(22) Shrestha, K. P.; Lhuillier, C.; Barbosa, A. A.; Brequigny, P.; Contino, F.; Mounaim-Rousselle, C.; Seidel, L.; Mauss, F. An Experimental and Modeling Study of Ammonia with Enriched Oxygen Content and Ammonia/Hydrogen Laminar Flame Speed at Elevated Pressure and Temperature. *Proc. Combust. Inst.* **2021**, *38*, 2163−2174.
(23) Chen, J.; Jiang, X.; Qin, X.; Huang, Z. Effect of Hydrogen Blending on the High Temperature Auto-Ignition of Ammonia at Elevated Pressure. *Fuel* **2021**, *287*, No. 119563.
(24) Tian, Z.; Li, Y.; Zhang, L.; Glarborg, P.; Qi, F. An Experimental and Kinetic Modeling Study of Premixed $NH_3/CH_4/O_2$/Ar Flames at Low Pressure. *Combust. Flame* **2009**, *156*, 1413−1426.
(25) Okafor, E. C.; Naito, Y.; Colson, S.; Ichikawa, A.; Kudo, T.; Hayakawa, A.; Kobayashi, H. Experimental and Numerical Study of the Laminar Burning Velocity of CH_4-NH_3-Air Premixed Flames. *Combust. Flame* **2018**, *187*, 185−198.
(26) Okafor, E. C.; Naito, Y.; Colson, S.; Ichikawa, A.; Kudo, T.; Hayakawa, A.; Kobayashi, H. Measurement and Modelling of the Laminar Burning Velocity of Methane-Ammonia-Air Flames at High Pressures using a Reduced Reaction Mechanism. *Combust. Flame* **2019**, *204*, 162−175.
(27) Dai, L.; Gersen, S.; Glarborg, P.; Mokhov, A.; Levinsky, H. Autoignition Studies of NH_3/CH_4 Mixtures at High Pressure. *Combust. Flame* **2020**, *218*, 19−26.
(28) Shu, B.; He, X.; Ramos, C. F.; Fernandes, R. X.; Costa, M. Experimental and Modeling Study on the Auto-Ignition Properties of Ammonia/Methane Mixtures at Elevated Pressures. *Proc. Combust. Inst.* **2021**, *38*, 261−268.
(29) Han, X.; Wang, Z.; He, Y.; Zhu, Y.; Cen, K. Experimental and Kinetic Modeling Study of Laminar Burning Velocities of NH_3/Syngas/Air Premixed Flames. *Combust. Flame* **2020**, *213*, 1−13.
(30) Zhou, S.; Yang, W.; Tan, H.; An, Q.; Wang, J.; Dai, H.; Wang, X.; Wang, X.; Deng, S. Experimental and Kinetic Modeling Study on NH_3/Syngas/Air and NH_3/Bio-Syngas/Air Premixed Laminar Flames at Elevated Temperatures. *Combust. Flame* **2021**, *233*, No. 111594.
(31) Wang, Z.; Han, X.; He, Y.; Zhu, R.; Zhu, Y.; Zhou, Z.; Cen, K. Experimental and Kinetic Study on the Laminar Burning Velocities of NH_3 Mixing with CH_3OH and C_2H_5OH in Premixed Flames. *Combust. Flame* **2021**, *229*, No. 111392.
(32) Han, X.; Lavadera, M. L.; Konnov, A. A. An Experimental and Kinetic Modeling Study on the Laminar Burning Velocity of NH_3+N_2O+Air Flames. *Combust. Flame* **2021**, *228*, 13−28.
(33) Lindstedt, R. P.; Lockwood, F. C.; Selim, M. A. Detailed Kinetic Modelling of Chemistry and Temperature Effects on Ammonia Oxidation. *Combust. Sci. Technol.* **1994**, *99*, 253−276.
(34) Gehring, M.; Hoyermann, K.; Schacke, H.; Wolfrum, J. Direct Studies of Some Elementary Steps for the Formation and Destruction of Nitric Oxide in the H-N-O System. *Proc. Combust. Inst.* **1973**, *14*, 99−105.
(35) Dransfeld, P.; Hack, W.; Kurzke, H.; Temps, F.; Wagner, H. G. Direct Studies of Elementary Reactions of NH_2 Radicals in the Gas Phase. *Proc. Comb. Inst.* **1985**, *20*, 655−663.
(36) Adamson, J. D.; Farhat, S. K.; Morter, C. L.; Glass, G. P.; Curl, R. F.; Phillips, L. F. The Reaction of NH_2 with O. *J. Phys. Chem. A* **1994**, *98*, 5665−5669.
(37) Inomata, S.; Washida, N. Rate Constants for the reactions of NH_2 and HNO with Atomic Oxygen at Temperatures Between 242 and 473 K. *J. Phys. Chem. A* **1999**, *103*, 5023−5031.
(38) Patel-Misra, D.; Dagdigian, P. J. Dynamics of the $O(^3P)$ + NH_2 Reaction: The HNO + H Product Channel. *Chem. Phys. Lett.* **1991**, *185*, 387−392.
(39) Patel-Misra, D.; Sauder, D. G.; Dagdigian, P. J. Internal State Distribution of OD Produced from the $O(^3P)$ + ND_2 Reaction. *J. Chem. Phys.* **1991**, *95*, 955−962.
(40) Dodonov, A. F.; Zelenov, V. V.; Strunin, V. P.; Tal'roze, V. L. Mass Spectrometic Determination of Rate Constants of Reaction Steps. VII. Flow Rate and Contact Time in the Mass Spectrometric Probing of a Diffusional Cloud in a Flow. *Kinet. Catal.* **1981**, *22*, 689.
(41) Bulewicz, E. M.; Sugden, T. M. Flame Photometric Studies of Reactions Induced by Nitric Oxide in Hydrogen-Oxygen-Nitrogen Flames. I. The Catalyzed Recombination of Atomic Hydrogen and Hydroxyl Radical. *Proc. R. Soc. London A* **1964**, *277*, 143−154.
(42) Halstead, C. J.; Jenkins, D. R. Catalysis of Recombination Reactions in Flames by Nitric Oxide. *Chem. Phys. Lett.* **1968**, *2*, 281−282.
(43) Smith, M. Y. The Effect of Nitric Oxide on the Recombination of H Atoms in Fuel-Rich Propane-Oxygen-Nitrogen Flames. *Combust. Flame* **1972**, *18*, 293−295.
(44) Ando, H.; Asaba, T. Rate Constants of Elementary Reactions in the High Temperature System of Nitric Oxide and Hydrogen. *Int. J. Chem. Kinet.* **1976**, *8*, 259−275.
(45) Koshi, M.; Ando, H.; Oya, M.; Asaba, T. Shock Tube Study of Decomposition of Nitric Oxide at High Temperatures. *Proc. Combust. Inst.* **1975**, *15*, 809−822.
(46) Natarajan, K.; Mick, H. J.; Woiki, D.; Roth, P. A Shock Tube Study of the Reaction H_2 + NO → HNO + H. *Combust. Flame* **1994**, *99*, 610−616.
(47) Kovacs, M.; Papp, M.; Zsely, I. G.; Turanyi, T. Determination of Rate Parameters of Key N/H/O Elementary Reactions Based on H_2/O_2/NOx Combustion Experiments. *Fuel* **2020**, *264*, No. 116720.
(48) Bozzelli, J. W.; Dean, A. M. Energized Complex Quantum Rice-Ramsperger-Kassel Analysis on Reactions of NH_2 with HO_2, O_2, and O Atoms. *J. Phys. Chem.* **1989**, *93*, 1058−1065.
(49) Walch, S. P. Theoretical Characterization of the Reaction NH_2 + O → Products. *J. Chem. Phys.* **1993**, *99*, 3804−3808.
(50) Yang, D. L.; Koszykowski, M. L.; Durant, J. L. The Reaction of NH_2 (X^2B_1) with O (X^3P): A Theoretical Study Employing Gaussian 2 Theory. *J. Chem. Phys.* **1994**, *101*, 1361−1368.
(51) Duan, X. F.; Page, M. Ab Initio Variational Transition State Theory Calculations for the O + NH_2 Hydrogren Abstraction Reaction on the 4A' and 4A″ Potential Energy Surface. *J. Chem. Phys.* **1995**, *102*, 6121−6127.
(52) Soto, M. R.; Page, M. Ab Initio Variational Transition State Theory Reaction-Rate Calculations for the Gas-Phase Reaction H + HNO → H_2 + NO. *J. Chem. Phys.* **1992**, *97*, 7287−7296.
(53) Page, M.; Soto, M. R. Radical Addition to HNO. Ab Initio Reaction Path and Variational Transition State Theory Calculations for H + HNO → H_2NO and H + HNO → HNOH. *J. Chem. Phys.* **1993**, *99*, 7709−7717.
(54) Nguyen, H. M. T.; Zhang, S.; Peeters, J.; Truong, T. N.; Nguyen, M. T. Direct Ab Initio Dynamics Studies of the Reactions of HNO with H and OH radicals. *Chem. Phys. Lett.* **2004**, *388*, 94−99.
(55) Klippenstein, S. J.; Harding, L. B.; Ruscic, B.; Sivaramakrishnan, R.; Srinivasan, N. K.; Su, M.-C.; Michael, J. V. Thermal Decomposition of NH_2OH and Subsequent Reactions: Ab Initio Transition State Theory and Reflected Shock Tube Experiments. *J. Phys. Chem. A* **2009**, *113*, 10241−10259.

https://doi.org/10.1021/acs.jpca.3c05181
J. Phys. Chem. A 2023, 127, 8650−8662

(56) Vessally, E.; Ebrahimi, S.; Goodarzi, M.; Seif, A. Insight into Detailed Mechanism of the Atmospheric Reaction of Imidogen with Hydroxyl: A Computational Study. *Struct. Chem.* **2014**, *25*, 169−175.
(57) Sharafdini, R.; Ramazani, S. Dynamic and Kinetic Parameters and Energy Exchanges of Particles in Reaction of NH + OH and Deuterated Analogues on an Interpolated Potential Energy Surface. *Chem. Sel.* **2020**, *5*, 3518−3528.
(58) Asemani, S. S.; Mousavipour, S. H. Dynamics of Imidogen Reaction with Hydroxyl Radical: A Theoretical Approach. *J. Iran. Chem. Soc.* **2020**, *17*, 1987−2000.
(59) Homayoon, Z.; Bowman, J. M. A Global Potential Energy Surface Describing the $N(^2D) + H_2O$ Reaction and a Quasiclassical Trajectory Study of the Reaction to NH + OH. *J. Phys. Chem. A* **2014**, *118*, 545−553.
(60) Kurosaki, Y.; Takayanagi, T. Ab Initio Molecular Orbital Study of the $N(^2D) + H_2O$ Reaction. *J. Phys. Chem. A* **1999**, *103*, 436−442.
(61) Isegawa, M.; Liu, F.; Maeda, S.; Morokuma, K. Complete Active Space Second Order Perturbation Theory (CASPT2) study of $N(^2D) + H_2O$ Reaction Paths on D_1 and D_0 Potential Energy Surfaces: Direct and Roaming Pathways. *J. Chem. Phys.* **2014**, *141*, No. 154303.
(62) Kurosaki, Y.; Takayanagi, T. Ab Initio Molecular Orbital Study of Potential Energy Surface for the $H_2NO\ (^2B_1) \rightarrow NO(^2\Pi) + H_2$ Reaction. *J. Mol. Struct.* **2000**, *507*, 119−126.
(63) Sumathi, R.; Sengupta, D.; Nguyen, M. T. Theoretical Study of the H_2 + NO and Related Reactions of $[H_2NO]$ Isomers. *J. Phys. Chem. A* **1998**, *102*, 3175−3183.
(64) Klippenstein, S. J. From Theoretical Reaction Dynamics to Chemical Modeling of Combustion. *Proc. Combust. Inst.* **2017**, *36*, 77−111.
(65) Klippenstein, S. J.; Harding, L. B.; Ruscic, B. Ab Initio Computations and Active Thermochemical Tables Hand in Hand: Heats of Formation of Core Combustion Species. *J. Phys. Chem. A* **2017**, *121*, 6580−6602.
(66) Woon, D. E.; Dunning, T. H. Gaussian-Basis Sets for Use in Correlated Molecular Calculations. 5. Core-Valence Basis-sets for Boron through Neon. *J. Chem. Phys.* **1995**, *103*, 4572−4585.
(67) Kállay, M.; Gauss, J. Approximate Treatment of Higher Excitations in Coupled-Cluster Theory. *J. Chem. Phys.* **2005**, *123*, No. 214105.
(68) Peng, D.; Reiher, M. Exact Decoupling of the Relativistic Fock Operator. *Theor. Chem. Acc.* **2012**, *131*, 1081.
(69) Handy, N. C.; Yamaguchi, Y.; Schaefer, H. F. The Diagonal Correction to the Born Oppenheimer Approximation − Its Effect on the Singlet-Triplet Splitting of CH_2 and other Molecular Effects. *J. Chem. Phys.* **1986**, *84*, 4481−4484.
(70) Grimme, S.; Antony, J.; Ehrlich, S.; Krieg, H. A Consistent and Accurate Ab Initio Parameterization of Density Functional Dispersion Correction (DFT-D) for the 94 elements H-Pu. *J. Chem. Phys.* **2010**, *132*, No. 154104.
(71) Knizia, G.; Adler, T. B.; Werner, H.-J. Simplified CCSD(T)-F12 Methods: Theory and Benchmarks. *J. Chem. Phys.* **2009**, *130*, No. 054104.
(72) Peterson, K. A.; Adler, T. B.; Werner, H.-J. Systematically Convergent Basis Sets for Explicitly Correlated Wavefunctions: The Atoms H, He, B-Ne, and Al-Ar. *J. Chem. Phys.* **2008**, *128*, No. 084102.
(73) Peterson, K. A.; Kesharwani, M. K.; Martin, J. M. L. The cc-pV5Z-F12 Basis Set: Reaching the Basis Set Limit in Explicitly Correlated Calculations. *Mol. Phys.* **2015**, *113*, 1551−1557.
(74) Werner, H.-J.; Knowles, P. J.; Knizia, G.; Manby, F. R.; Schutz, M.; Celani, P.; Gyorffy, W.; Kats, D.; Korona, T.; Lindh, R.; Mitrushenkov, A.; Rauhut, G.; Shamasundar, K. R.; Adler, T. B.; Amos, R. D.; Bernhardsson, A.; Berning, A.; Cooper, D. L.; Deegan, M. J. O.; Dobbyn, A. J.; Eckert, F.; Goll, E.; Hampel, C.; Hesselmann, A.; Hetzer, G.; Hrenar, T.; Jansen, G.; Koppl, C.; Liu, Y.; Lloyd, A. W.; Mata, R. A.; May, A. J.; McNicholas, S. J.; Meyer, W.; Mura, M. E.; Nicklass, A.; O'Neill, D. P.; Palmieri, P.; Peng, D.; Pfluger, K.; Pitzer, R.; Reiher, M.; Shiozaki, T.; Stoll, H.; Stone, A. J.; Tarroni, R.; Thorsteinsson, T.; Wang, M. *MOLPRO*, version 2015.1, a package of ab initio programs; http://www.molpro.net; accessed 7-21-2023.
(75) Werner, H.-J.; Knowles, P. J.; Knizia, G.; Manby, F. R.; Schutz, M. Molpro: A General-Purpose Quantum Chemistry Program Package. *WIREs Comput. Mol. Sci.* **2012**, *2*, 242−253.
(76) Stanton, J. F.; Gauss, J.; Harding, M. E.; Szalay, P. G. with contributions from Auer, A. A.; Bartlett, R. J.; Benedikt, U.; Berger, C.; Bernholdt, D. E.; Bomble, Y. J., et al. and the integral packages MOLECULE (Almlof, J. P; Taylor, R.), PROPS (Taylor, P. R.), ABACUS (Helgaker, T.; Jensen, H. J.; Jørgensen, P.; Olsen, J.), and ECP routines by Mitin, A. V.; van Wüllen, C. For the current version, see http://www.cfour.de; accessed 7-21-2023.
(77) MRCC, A String-Based Quantum Chemical Program Suite written by Kállay, M. See also Kállay, M.; Surján, P. R. Higher Excitations in Coupled-Cluster Theory. *J. Chem. Phys.* **2001**, *115*, 2945−2954.
(78) Frisch, M. J.; Trucks, G. W.; Schlegel, H. B.; Scuseria, G. E.; Robb, M. A.; Cheeseman, J. R.; Scalmani, G.; Barone, V.; Mennucci, B.; Petersson, G. A.; et al. *Gaussian 09*, Revision D.01; Gaussian, Inc.: Wallingford, CT, 2009.
(79) Klippenstein, S. J. Variational Optimizations in the RRKM Theory Calculations for Unimolecular Dissociations with No Reverse Barrier. *J. Chem. Phys.* **1992**, *96*, 367−371.
(80) Georgievskii, Y.; Klippenstein, S. J. Transition State Theory for Multichannel Addition Reactions: Multifaceted Dividing Surfaces. *J. Phys. Chem. A* **2003**, *107*, 9776−9781.
(81) Klippenstein, S. J.; Georgievskii, Y.; Harding, L. B. Statistical Theory for the Kinetics and Dynamics of Roaming Reactions. *J. Phys. Chem. A* **2011**, *115*, 14370−14381.
(82) Moradi, C. P.; Morrison, A. M.; Klippenstein, S. J.; Goldsmith, C. F.; Douberly, G. E. Propargyl + O_2 Reaction in Helium Droplets: Entrance Channel Barrier or Not? *J. Phys. Chem. A* **2013**, *117*, 13626−13635.
(83) Klippenstein, S. J.; Georgievskii, Y.; Harding, L. B. Predictive Theory for the Combination Kinetics of Two Alkyl Radicals. *Phys. Chem. Chem. Phys.* **2006**, *8*, 1133−1147.
(84) Georgievskii, Y.; Klippenstein, S. J. Long-Range Transition State Theory. *J. Chem. Phys.* **2005**, *122*, No. 194103.
(85) Georgievskii, Y.; Miller, J. A.; Burke, M. P.; Klippenstein, S. J. Reformulation and Solution of the Master Equation for Multiple-Well Chemical Reactions. *J. Phys. Chem. A* **2013**, *117*, 12146−12154.
(86) https://github.com/Auto-Mech/MESS; accessed 7-21-2023.
(87) Ruscic, B.; Pinzon, R. E.; Morton, M. L.; von Laszevski, G.; Bittner, S. J.; Nijsure, S. G.; Amin, K. A.; Minkoff, M.; Wagner, A. F. Introduction to Active Thermochemical Tables: Several "Key" Enthalpies of Formation Revisited. *J. Phys. Chem. A* **2004**, *108*, 9979−9997.
(88) https://atct.anl.gov/ version TN 1.124; accessed 7-21-2023.
(89) Klippenstein, S. J.; Harding, L. B.; Glarborg, P.; Miller, J. A. The Role of NNH in NO Formation and Control. *Combust. Flame* **2011**, *158*, 774−789.
(90) Miller, J. A.; Smooke, M. D.; Green, R. M.; Kee, R. J. Kinetic Modeling of the Oxidation of Ammonia in Flames. *Combust. Sci. Technol.* **1983**, *34*, 149−176.
(91) Dagaut, P. On the Oxidation of Ammonia and Mutual Sensitization of the Oxidation of NO and Ammonia: Experimental and Kinetic Modeling. *Combust. Sci. Technol.* **2022**, *194*, 117−129.
(92) Duo, W. Kinetic Studies of the Reactions Involved in Selective Non-Catalytic Reduction of Nitric Oxide. Ph.D. Thesis. DTU Chemical Engineering, Technical University of Denmark, 1990.

https://doi.org/10.1021/acs.jpca.3c05181
J. Phys. Chem. A 2023, 127, 8650−8662